Adaptive Meshless Methods in Electromagnetic Modeling: A Gradient-Based Refinement Strategy

Thomas Kaufmann [#1], Christian Engström [*2], Christophe Fumeaux [#3]

[#] *School of Electrical & Electronic Engineering, The University of Adelaide*
Adelaide, South Australia 5005, Australia
[1] thomaska@eleceng.adelaide.edu.au
[3] cfumeaux@eleceng.adelaide.edu.au

[*] *Laboratory for Electromagnetic Fields and Microwave Electronics (IFH), ETH Zurich,*
Gloriastrasse 35, Zurich, CH-8092, Switzerland
[2] christian.engstrom@ifh.ee.ethz.ch

***Abstract*— Meshless methods are numerical methods that have the advantage of high accuracy without the need of an explicitly described mesh topology. In this class of methods, the Radial Point Interpolation Method (RPIM) is a promising collocation method where the application of radial basis functions yields high interpolation accuracy for even strongly unstructured node distributions. For electromagnetic simulations in particular, this distinguishing characteristic translates into an enhanced capability for conformal and multi-scale modeling. The method also facilitates adaptive discretization refinements, which provides an important tool to decrease memory consumption and computation time. In this paper, a refinement strategy is introduced for RPIM. In the proposed node adaptation algorithm, the accuracy of a solution is increased iteratively based on an initial solution with a coarse discretization. In contrast to the commonly used residual-based adaptivity algorithms, this definition is extended by an error estimator based on the solution gradient. In the studied cases this strategy leads to increased convergence rates compared with the standard algorithm. Numerical examples are provided to illustrate the effectiveness of the algorithm.**

I. Introduction

Meshless methods have recently attracted interest recently in computational modeling across various engineering disciplines due to their striking properties [1]. This novel class of numerical algorithms provides the ability of conformal and multi-scale modeling with an unstructured node distribution without the need of defining an explicit mesh topology. For electromagnetic modeling, instead of solving the Maxwell's equations on a mesh structure, a solution is sought on arbitrarily located nodes in a collocation approach. This facilitates conformal modeling of complex structures and dynamic adaptation of node distributions. Using radial basis functions (RBF), a very high interpolation accuracy can be achieved with a low number of nodes. The radial point interpolation method (RPIM) [2] is a prominent representative of meshless methods based on RBFs, and is used throughout this paper. Theoretical evaluations have shown that exponential convergence rates can be achieved either through a refined node distribution, or through the flattening of the radial basis functions [3].

In the framework of RBF-based meshless methods, generally two approaches exist. First, for very high accuracy, global basis functions extend over the whole computational domain. They attractive for small problems and for achieving very high accuracy. Unfortunately, in this approach the solution requires the inversion of a full matrix for the domain considered and the computational effort rises quickly with the size of the problem. A remedy to this issue is provided by domain decomposition methods, where the computational domain is split into several subdomains, each of which can be solved separately very efficiently. In an iterative approach, a global solution can be found by "stitching" solutions of the sub-domains, e.g. using a Schwartz scheme [4]. An alternative approach is the use of local basis functions, where only nodes in a small support domain encircling each node are considered. This local approach results in efficient solutions based on sparse matrices, however at the cost a degradation of interpolation accuracy.

In the context of computational electromagnetics, several important steps of RPIM implementations have recently been presented. A time-domain solver based on a local formulation has been introduced in [5] for a two-dimensional formulation and extended in [6] to three-dimensional problems. Spectral properties of the method and longtime stability issues have been presented in [7]. Alternative approaches towards unconditionally stable formulations were published [8] with an alternating-direction-implicit (ADI) formulation that allowed time steps much larger than the classical Courant-Friedrich-Levy (CFL) limit. Later, an extension using Laguerre basis functions to model the time evolution has been presented [9].

For resonant cavities, an RPIM solver using global basis functions has been introduced in [10] with a comparison to other RBF methods. For that solver, a residual-based refinement algorithm has been introduced in [11]. In the present publication, this refinement strategy is extended with a gradient-based a posteriori error estimator.

II. Interpolation Algorithm

The approximation of a field component u at position $\mathbf{x} = (x, y)^T$ is expressed through the following linear combination of RBFs

$$u(\mathbf{x}) \approx \langle u(\mathbf{x}) \rangle = \sum_{i=1}^{N} r_n(\mathbf{x}) a_n = \mathbf{r}(\mathbf{x})\mathbf{a}. \qquad (1)$$

The RBFs selected here are of Gaussian type as they are known for their excellent interpolation quality. The basis

functions are centered at collocation node location $\mathbf{x}_n$, i.e.

$$r_n(\mathbf{x}) = \exp\left(-\alpha_c \frac{|\mathbf{x}_n - \mathbf{x}|^2}{d_c}\right) \tag{2}$$

and contain a shape parameter α_c and a normalization factor d_c denoting the average node distance. As investigated in [7], widening the shape of the RBF by lowering the shape parameter α_c improves the interpolation accuracy until a numerical limit for the condition number of the matrices is reached.

Optionally, the basis can be expanded with additional basis functions: monomial functions proved to be advantageous to interpolate linear functions [2], and singular functions helped significantly improve the performance for singular problems [12] in computational mechanics.

The interpolation parameter $\mathbf{a} = (a_1, \ldots, a_N)$ is calculated in a preprocessing step using a point-matching procedure. Expressing the interpolation of the field component u at all collocation nodes allows the setup of a linear system

$$\begin{pmatrix} u(\mathbf{x}_1) \\ \vdots \\ u(\mathbf{x}_N) \end{pmatrix} = \begin{pmatrix} r_1(\mathbf{x}_1) & \ldots & r_N(\mathbf{x}_1) \\ \vdots & \ddots & \vdots \\ r_N(\mathbf{x}_1) & \ldots & r_N(\mathbf{x}_N) \end{pmatrix} \begin{pmatrix} a_1 \\ \vdots \\ a_N \end{pmatrix} \tag{3}$$

$$\mathbf{u}^e = \mathbf{R}_0 \mathbf{a}. \tag{4}$$

A set of shape functions is calculated from

$$\langle u(\mathbf{x}) \rangle = \mathbf{r}^T(\mathbf{x})\mathbf{a} = \mathbf{r}^T(\mathbf{x})\mathbf{R}_0^{-1}\mathbf{u}^e = \mathbf{\Psi}(\mathbf{x})\mathbf{u}^e. \tag{5}$$

Based on this expression, the approximations of l^{th}-order spatial derivatives along $\kappa = x, y$ can be derived straightforwardly

$$\left\langle \partial_\kappa^l u(\mathbf{x}) \right\rangle = \partial_\kappa^l \mathbf{r}^T(\mathbf{x})\mathbf{R}_0^{-1}\mathbf{u}^e = \partial_\kappa^l \mathbf{\Psi}(\mathbf{x})\mathbf{u}^e. \tag{6}$$

The interpolation accuracy is improved by selecting a low value of the shape parameter α_c, which however increases the matrix condition number of $\mathbf{R}_0$. Best results are achieved close to the limit of the numerical stability. A numerical optimization called "leave-one-out-cross-validation" (LOOCV) [13] assists the automatic selection of a nearly optimal value of α_c. An interesting alternative to this strategy is an adaptation of the Gaussian basis functions to obtain high accuracy for low values of the shape parameter [14].

III. Eigenvalue Solver

Eigenvalue solvers for meshless RBF methods have been presented for the compactly supported Wendland functions in [15] and [16]. An eigenvalue solver for the RPIM variant of RBF methods has been previously introduced in [10] and compared with other RBF methods. The algorithm is therefore only briefly summarized here.

In contrast to the usual RBF methods, the RPIM algorithm solves directly for the field components. In this paper, a 2D setup for resonant cavities computes the TM modes of given structures, i.e. the E_z component. The governing eigenvalue problem is based on the source-free second-order Helmholtz equation

$$-\Delta E_z - k^2 E_z = 0, \tag{7}$$

where we solve for the eigenvalues $\lambda = k^2$

$$-\Delta E_z = \lambda E_z. \tag{8}$$

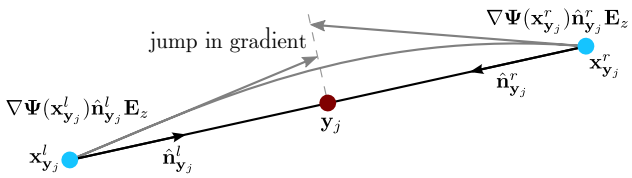

Fig. 1. A posteriori estimator of jump in gradient between left ($\mathbf{x}^l_{\mathbf{y}_j}$) and right ($\mathbf{x}^r_{\mathbf{y}_j}$) neighbor of test node $\mathbf{y}_j$.

The spatial domain is discretized using an unstructured collocation node distribution $\mathbf{x}_1, \ldots, \mathbf{x}_{N_I}, \mathbf{x}_{N_I+1}, \ldots, \mathbf{x}_{N_I+N_B}$ with N_I interior and N_B boundary nodes. The boundaries are assumed to be of Dirichlet type

$$E_z = 0, \tag{9}$$

which corresponds to a perfect electric conductor (PEC). The Laplace operator is approximated through (6) and the collocation problem is formulated as follows on the interior nodes [10]

$$-\Delta\mathbf{\Psi}\mathbf{E}_z = \lambda\mathbf{\Psi}\mathbf{E}_z. \tag{10}$$

The vectors $\mathbf{E}_z$ of length N_I represent the eigenvectors quadratic stiffness matrix. The eigenvalues are computed with the general purpose package LAPACK [17].

IV. Node Adaptivity

Based on a given collocation node distribution, a set of test nodes $\mathbf{y}_1, \ldots, \mathbf{y}_{N_T}$ is obtained through a Delaunay tessellation [18]. The test nodes are placed on the edge centers of the Delaunay triangles. This assures an even node distribution at intermittent locations of the collocation nodes. On these test node locations, an estimated a posteriori error is calculated. The previously introduced residual form of the estimated error [11] is enhanced here with an estimation of the jump in the gradient of the previous solution (Fig. 1). Inspired by the finite element approach [19], where the jump of the gradient between two mesh cells is estimated, high values of this estimator indicates rapid field variations. The error estimator is expressed as the weighted sum of three terms

$$\eta(\mathbf{y}_j) = \begin{cases} \nu_1 d^2_{\mathbf{y}_j} |\Delta\mathbf{\Psi}(\mathbf{y}_j)\mathbf{E}_z + \lambda\mathbf{\Psi}(\mathbf{y}_j)\mathbf{E}_z|^2 \text{ in bulk} & \text{(a)} \\ +\nu_2 d^2_{\mathbf{y}_j} |\mathbf{\Psi}(\mathbf{y}_j)\mathbf{E}_z|^2 \text{ on PEC} & \text{(b)} \\ +\nu_3 d^2_{\mathbf{y}_j} |\nabla\mathbf{\Psi}(\mathbf{x}^l_{\mathbf{y}_j})\mathbf{E}_z\hat{\mathbf{n}}^l_{\mathbf{y}_j} + \nabla\mathbf{\Psi}(\mathbf{x}^r)\mathbf{E}_z\hat{\mathbf{n}}^r_{\mathbf{y}_j}|^2 & \text{(c)} \end{cases} \tag{11}$$

with $d_{\mathbf{y}_j}$ representing the distance between the corresponding left ($\mathbf{x}^l_{\mathbf{y}_j}$) and right ($\mathbf{x}^r_{\mathbf{y}_j}$) neighbors of test node $\mathbf{y}_j$. The terms (a) and (b) represent the residual-based error estimator in the interior and on the PEC boundary, respectively. The new part, the estimation of the jump in the gradient, is shown in (c). Weighting factors are applied to account for the different scales of the errors. Numerical experiments show that a good choice of the factors is $\nu_1 = 1, \nu_2 = 500, \nu_3 = 0.1$, even though the choice is rather robust, as previously reported in [11]. The shape functions in (11) are calculated on the test node locations based on (5) and (6).

The adaptivity strategy is applied iteratively. In each iteration step the error estimator (11) is calculated and all test nodes with an estimated error larger than

$$\eta(\mathbf{y}_j) \geq \beta \max_i \eta(\mathbf{y}_i), \tag{12}$$

are added to the set of collocation nodes. The threshold parameter β is typically chosen as $\beta = 0.35$. At each step, the LOOCV algorithm is applied to find an optimized shape parameter α_c. The iteration is performed until the required level of accuracy is reached. As an indicator of the overall error, either the change in the solution between the iterations can be taken into account, or a global error estimator

$$\eta_g = \sum_{j=1}^{N_T} \eta(\mathbf{y}_j) \tag{13}$$

can be applied.

In the following, the new extended adaptive refinement algorithm is illustrated on a numerical example.

V. Numerical Illustration

Numerical experiments are performed on a rectangular cavity. The size in normalized units is chosen as 1.5×1. The eigenmodes of this structure are calculated and the relative eigenvalue errors in comparison with the analytical results [20]

$$\epsilon_{rel} = \frac{\lambda - k^2}{k^2} \tag{14}$$

are recorded for each mode and each node arrangement.

In a first step, the evolution of the adaptive refinement algorithm is illustrated on the TM_{12}-mode. An initial solution is calculated with a very coarse node distribution consisting of only $N_I = 6$ interior and $N_B = 14$ boundary nodes. Then a set of test nodes is constructed, and the relative error (11) is estimated based on the initial solution. Fig. 2a shows the estimated error as cells around each test node. Nodes with an error larger than the threshold (12) are subsequently added to the set of collocation nodes. Again, a solution is calculated based on this new set of nodes. Fig. 2b and 2c show the estimated error distribution at the second and fourth iteration step. After five iterations, the error (14) is lower than 10^{-6}. The corresponding node and field distribution is shown in Fig. 2d. Slight asymmetries can be observed in the final node distribution. They arise from the arbitrary choice of the threshold parameter β, meaning that in certain situation the nodes with estimated errors close to the threshold might not be added due to roundoff errors. It could be observed though that the node densities generally remain symmetric, with slight variations in the details.

In a second step, the refinement of the TM_{12} and TM_{21} mode is performed on the rectangular structure. The relative eigenvalue error is compared to a uniform and a residual-based refinement strategy. Fig. 3 shows the results. In both cases, the new gradient-based refinement strategy (11) is superior to the other algorithms. The advantage is clearer in the TM_{12}-case due to the steeper changes in the gradients of the solution (s. Fig. 2d). It should be noted though that the error decreases at a very large rate for all refinement strategies - the relative

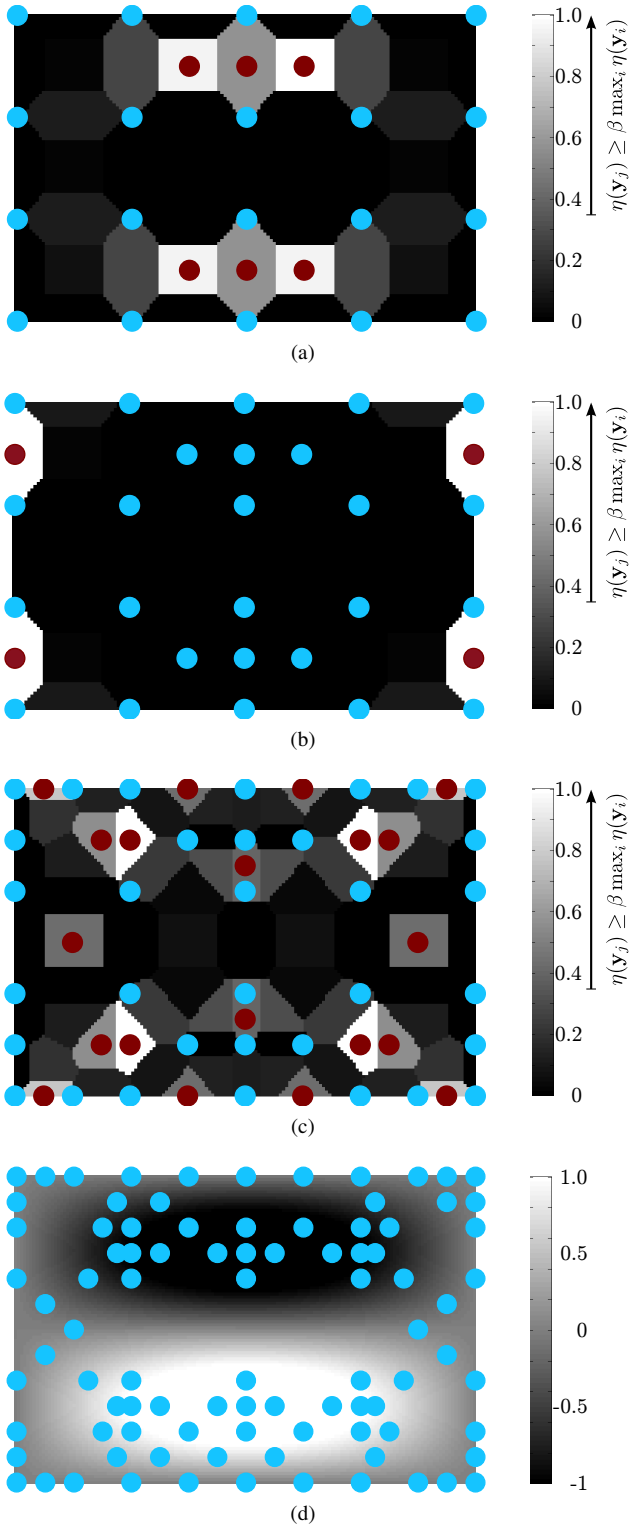

Fig. 2. Estimated errors $\eta(\mathbf{y}_j)$ at the first (a), second (b) and fourth (c) iteration step for the TM_12 mode the collocation nodes are shown as blue dots, and the newly added nodes are shown as red dots. The last figure (d) shows the final node and field distribution E_z to yield a relative eigenvalue error of $< 10^{-6}$.

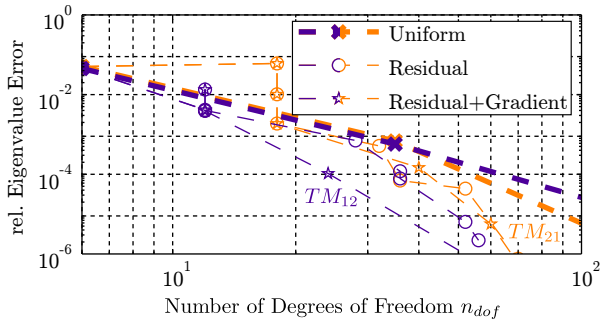

Fig. 3. Eigenvalue error for the TM_{12} and TM_{21} mode of a rectangular cavity. Comparison between a uniform refinement, residual-based and the proposed residual-based extended with the gradient-based adaptive refinement algorithms.

eigenvalue error is below 10^{-4} for less than $n_{dof} = 60$ degrees of freedom. The calculation time of the LAPACK solver in that case is less than 5 ms on a standard PC.

VI. Conclusion

Meshless methods build a promising class of numerical modeling techniques for electromagnetics because of the possibility of conformal and multiscale modeling capabilities without the need of an explicit mesh topology. Due to the excellent interpolation properties of the applied radial basis functions very accurate results can be achieved for relatively short computation times. This paper has first reviewed the current state of the art of the RPIM method, as meshless collocation solver for electromagnetic problem.

One of the most attractive feature of meshless method is provided by the possibility to add, move or remove nodes of the discretization. This opens new possibilities for optimization, and adaptive discretization of problems, both in time and frequency domain. In this perspective, a new gradient-based refinement strategy has been introduced in this paper. The proposed iterative refinement algorithm has been demonstrated in the framework of an RPIM eigenvalue solver. Based on a previous solution on a coarse grid, an error is estimated on a secondary set of test locations. Test nodes with a large error are then added to the set of collocation nodes. The new error estimator contains a residual-based indicator and an indicator based on the jump of the gradient between two collocation nodes. This second estimator allows to identify regions with rapid field variations. Numerical evaluations showed the effectiveness of this extended refinement strategy.

Even though the refinement algorithm is formulated for the RPIM scheme, it can be easily be adapted to other meshless collocation eigenvalue solvers and to source problems. Other possible applications of the presented error estimator are for a time-domain method to dynamically adapt a node distribution as a pulse propagates through a structure. The extended node refinement algorithm is an important step in the development of highly efficient and flexible meshless solvers in computational electromagnetics.

Acknowledgment

C. Fumeaux acknowledges the support of the Australian Research Council (ARC) Future Fellowship funding scheme (under FT100100585). T. Kaufmann was a PhD student at ETH Zurich when parts of this work was done.

References

[1] T. Belytschko, Y. Krongauz, D. Organ, M. Fleming, and P. Krysl, "Meshless methods: An overview and recent developments," *Computer Methods in Applied Mechanics and Engineering*, vol. 139, no. 1-4, pp. 3–47, 1996.

[2] G. Liu, *Mesh Free Methods: Moving Beyond the Finite Element Method*. Boca Raton, FL, USA: CRC Press, 2003.

[3] A. H.-D. Cheng, M. A. Golberg, E. J. Kansa, and G. Zammito, "Exponential convergence and H-c multiquadric collocation method for partial differential equations," *Numerical Methods for Partial Differential Equations*, vol. 19, no. 5, pp. 571–594, 2003.

[4] J. Li and Y. C. Hon, "Domain decomposition for radial basis meshless methods," *Numerical Methods for Partial Differential Equations*, vol. 20, no. 3, pp. 450–462, 2004.

[5] T. Kaufmann, C. Fumeaux, and R. Vahldieck, "The Meshless Radial Point Interpolation Method for Time-Domain Electromagnetics," in *IEEE MTT-S International Microwave Symposium Digest*. Atlanta, GA, USA: IEEE, June 2008, pp. 61–65.

[6] Y. Yu and Z. D. Chen, "A 3-D Radial Point Interpolation Method for Meshless Time-Domain Modeling," *IEEE Trans. Microwave Theory and Techn.*, vol. 57, no. 8, pp. 2015–2020, Aug. 2009.

[7] T. Kaufmann, C. Engström, C. Fumeaux, and R. Vahldieck, "Eigenvalue Analysis and Longtime Stability of Resonant Structures for the Meshless Radial Point Interpolation Method in Time Domain," *IEEE Trans. Microwave Theory and Techn.*, vol. 58, no. 12, pp. 3399–3408, December 2010.

[8] Y. Yu and Z. D. Chen, "An Unconditionally Stable Radial Point Interpolation Method for Efficient Meshless Modeling in Time Domain," in *25th Annual Review of Progress in ACES*, Monterey, USA, March 2009.

[9] X. Chen, Z. D. Chen, Y. Yu, and D. Su, "An Unconditionally Stable Radial Point Interpolation Meshless Method with Laguerre Polynomials," *IEEE Trans. Antennas and Propagation*, pp. 1–1, 2011, to be published.

[10] T. Kaufmann, C. Engström, and C. Fumeaux, "A Comparison of Three Meshless Algorithms: Radial Point Interpolation, Non-Symmetric and Symmetric Kansa MethodThe Meshless Radial Point Interpolation Method for Time-Domain Electromagnetics," in *IEEE MTT-S International Microwave Symposium Digest*. Baltimore, MD, USA: IEEE, June 2011, pp. 1–1, accepted for publication.

[11] ——, "Residual-Based Adaptive Refinement for Meshless Eigenvalue Solvers," in *International Conference in Electromagnetics on Advanced Applications*. Sydney, Australia: IEEE, Sept. 2010, pp. 244–247.

[12] M. Kindelan and F. Bernal, "Radial Basis Function (RBF) Solution of the Motz Problem," *Progress in Industrial Mathematics at ECMI 2008*, pp. 907–912, 2010.

[13] G. E. Fasshauer and J. Zhang, "On choosing "optimal" shape parameters for RBF approximation," *Numerical Algorithms*, vol. 45, no. 1, pp. 345–368, August 2007.

[14] B. Fornberg, E. Larsson, and N. Flyer, "Stable computations with gaussian radial basis functions," *SIAM Journal on Scientific Computing*, vol. 33, no. 2, pp. 869–892, 2011.

[15] P.-L. Jiang, S.-Q. Li, and C. H. Chan, "Analysis of elliptical waveguides by a meshless collocation method with the Wendland radial basis functions," *Microwave and Optical Technology Letters*, vol. 32, no. 2, pp. 162–165, 2002.

[16] P. Kowalczyk and M. Mrozowski, "Mesh-free approach to Helmholtz equation based on radial basis functions," *Journal of Telecommunications and Information Technology*, 2005.

[17] E. Anderson, Z. Bai, C. Bischof, S. Blackford, J. Demmel, J. Dongarra, J. D. Croz, A. Greenbaum, S. Hammarling, A. McKenney, and D. Sorensen, *LAPACK Users' Guide*, 3rd ed. Philadelphia, PA, USA: Society for Industrial and Applied Mathematics, 1999.

[18] B. B. T. Kee, G. R. Liu, G. Y. Zhang, and C. Lu, "A residual based error estimator using radial basis functions," *Finite Elements in Analysis and Design*, vol. 44, no. 9-10, pp. 631–645, 2008.

[19] M. Ainsworth and J. T. Oden, *A Posteriori Error Estimation in Finite Element Analysis*. New York, USA: John Wiley & Sons, Inc., September 2000.

[20] J. Jackson and R. Fox, "Classical electrodynamics," *American Journal of Physics*, vol. 67, 1999.